Applied Catalysis B: Environmental 241 (2019) 305–318

Contents lists available at ScienceDirect

Applied Catalysis B: Environmental

journal homepage: www.elsevier.com/locate/apcatb

Non-oxidative dehydroaromatization of methane over Mo/H-ZSM-5 catalysts: A detailed analysis of the reaction-regeneration cycle

Seung Ju Han[a], Seok Ki Kim[a,b], Ahron Hwang[a], Sungtak Kim[c], Do-Young Hong[a,b], Geunjae Kwak[a,b], Ki-Won Jun[a,b], Yong Tae Kim[a,b,*]

[a] Carbon Resources Institute, Korea Research Institute of Chemical Technology, Daejeon 34114, Republic of Korea
[b] Advanced Materials and Chemical Engineering, University of Science & Technology, Daejeon 34113, Republic of Korea
[c] Plant Engineering Division, Energy & Environment Research Team, Institute for Advanced Engineering, Yongin 17180, Republic of Korea

ARTICLE INFO

Keywords:
Methane dehydroaromatization
Mo/H-ZSM-5 catalyst
Regeneration process
Coke removal

ABSTRACT

Of several Mo/H-ZSM-5 catalysts (Mo loading = 1, 3, 5, 7 wt%), 5Mo/H-ZSM-5 (5 wt%) exhibited the best catalytic performance for methane conversion and benzene yield for methane dehydroaromatization at 700 °C. It was observed that deactivation of zeolite acid sites precedes deactivation of the Mo_2C sites. Increasing the number of accessible Mo carbide sites with minimizing isolated surface acid sites is required for high benzene selectivity and stability. Under oxidative conditions, bifunctional metal-acid sites were reversibly regenerated at 450 °C; at higher temperatures of 550–850 °C, irreversible deactivation was observed. The selective recovery of Brønsted acid sites near Mo sites other than isolated acid sites is sufficient to restore the catalytic activity in terms of benzene formation. Spectroscopic studies revealed that high-temperature oxidative regeneration induced $(MoO_4^{2-})_n$ oligomerization and subsequent carburization of bulk Mo carbide cluster. The 5Mo/H-ZSM-5 underwent MoO_3 sublimation and loss of Brønsted acidity during oxidative regeneration at 850 °C. Reductive regeneration required a temperature higher than 700 °C for coke removal, but resulted in thermal degradation of the catalyst. Theoretical calculations indicated that partial oxidation of coke precursor (i.e. naphthalene) at 450 °C was more favorable than its partial hydrogenation at 850 °C on the Mo clusters in ZSM-5 channel. Overall, oxidative regeneration at 450 °C can maintain high Mo_2C dispersion and efficient coke removal during 60 h of methane reaction.

1. Introduction

Recently, the abundance of natural gas resources has led to the conversion of methane into higher-margin performance chemicals [1,2]. However, the strong C—H bonds of methane (425 kJ/mol [3]), as well as its non-polar structure and high ionization energy, require temperatures exceeding 700 °C for its direct conversion. Oxidative conversion of methane helps the reaction to operate at much milder conditions [2]. Because it is much easier to cleave all four C—H bonds of methane than to selectively dissociate a single C—H bond at high temperatures [4], indirect conversion of methane through syngas has been investigated. Methane can be converted into hydrocarbons through an integrated process; for example, methane reforming for syngas production (i.e., H_2 and CO) at relatively high temperatures (700–1100 °C), followed by Fischer–Tropsch synthesis at lower temperatures (200–350 °C) [5,6]. However, such processes have several challenges that must be addressed to improve energy and carbon efficiency, especially at small scale [7]. By comparison, direct methane conversion routes are potentially more economical and environmentally friendly than indirect routes, despite their thermodynamic limitations [4,8,9].

Methane dehydroaromatization (MDA) has attracted increasing interest due to high selectivity for the aromatic compounds, particularly benzene. In 1993, Wang et al. first reported the direct conversion of methane into aromatic compounds under non-oxidative conditions over a molybdenum (Mo) catalyst supported on H-ZSM-5 [10]. Since then, a number of catalysts utilizing various metals and supports have been applied to MDA [11–16]. Among them, Mo-based catalysts have demonstrated the highest catalytic activity [1]. In particular, the majority of research has focused on Mo catalysts supported on H-ZSM-5, which remains one of the best candidate for MDA catalysis [1,9,17]. It is generally regarded that the Mo sites in Mo/H-ZSM-5 catalysts promote C—H activation of methane, while the acidic sites catalyze the formation of aromatic compounds [1,18,19].

* Corresponding author.
E-mail address: ytkim@krict.re.kr (Y.T. Kim).

https://doi.org/10.1016/j.apcatb.2018.09.042
Received 24 April 2018; Received in revised form 11 September 2018; Accepted 15 September 2018
Available online 16 September 2018
0926-3373/

Several attempts have been made to improve the catalytic activity of MDA over Mo/H-ZSM-5 catalysts [1,20–23]. For instance, adding a (post)-transition metal such as Ga or Fe to the catalyst has been used to enhance the Mo or acid site activity for better conversion [20–24]. Additionally, improved catalytic performance was reported by modifying the zeolite supports via desilication or proton substitution for superior interactions with the metal and acid sites [25,26].

Although the MDA reaction can synthesize aromatic compounds, most of the active sites on the Mo/ZSM-5 catalyst rapidly lose their initial activity during catalysis because carbonaceous species become deposited [27]. In order to enhance catalytic stability, much research has focused on co-feeding gases with methane. For example, it has been reported that the addition of CO/CO_2 and NO gases significantly enhanced the catalytic stability of Mo/ZSM-5 by suppressing coke formation [12,28,29]. Co-feeding H_2 with methane is a simple and effective way to suppress coke formation; however, depending on the H_2 concentration, this approach shifts the thermodynamic equilibrium to lower methane conversion [30,31]. It is therefore of great interest to characterize how the spent catalyst reversibly restores its catalytic active sites. In this regard, the selective conversion of coke species deposited on the catalyst through O_2 [27,32] or H_2 [33–35] treatment has been shown to improve catalyst stability. Oxidative regeneration can effectively remove coke at low temperatures, but induces irreversible deactivation because of aluminum molybdate formation [27]. Combining a short reaction period with shortened oxidative regeneration step enhances the long-term stability of Mo/ZSM-5 catalyst [27,36]. These problems can be avoided in reductive regeneration processes, but this strategy has the disadvantage that it requires a high regeneration temperature [32,37]. Since there is no comparative study on the detailed effects of reductive and oxidative regeneration of Mo/ZSM-5 catalysts applied to the MDA reaction, a systematic investigation on both processes is required.

To this end, the purpose of this study is to understand the catalytic reaction chemistry for methane conversion over Mo/H-ZSM-5 catalysts. The catalysts were characterized before and after the reaction to elucidate the performance of the bifunctional catalytic systems. Reaction measurements of the Mo/H-ZSM-5 catalysts were performed to identify the differences in the regenerability of the reaction-regeneration steps. The results from this study may be useful to designing more effective catalysts and processes for the production of aromatic compounds from methane by MDA.

2. Experimental

2.1. Preparation of the Mo/H-ZSM-5 catalysts

Mo/H-ZSM-5 catalysts were prepared by a conventional wet impregnation method. Parent H-ZSM-5 was obtained by calcination of the purchased NH_4-ZSM-5 (SiO_2/Al_2O_3 = 30, 3024E, Zeolyst) at 600 °C for 2 h to convert NH^{4+} into H^+ before impregnation. Ammonium heptamolybdate ($(NH_4)_6Mo_7O_{24}{\cdot}4H_2O$, Samchun) was used as the Mo precursor. The Mo content used in the catalysts was 1–7 wt%, which is denoted as X in XMo/H-ZSM-5. After Mo impregnation, the impregnated powder was dried at 80 °C following calcination at 500 °C for 4 h.

2.2. Characterization

Adsorption and desorption isotherms of nitrogen were obtained for all of the samples at −196 °C using an ASAP 2020 system (Micromeritics). The catalyst surface area was calculated using the BET equation. The average pore diameter of each catalyst was calculated by the Barrett–Joyner–Halenda (BJH) desorption method. The total pore volume was determined at a relative pressure (P/P_0) of 0.99. Before the measurements, the samples were degassed under vacuum at 300 °C for 12 h.

The bulk crystalline structures of the catalysts were determined by X-ray diffraction (XRD) using an Ultima IV diffractometer (Rigaku) with Cu Kα radiation (λ = 0.15406 nm), operated at 40 kV and 40 mA. The crystalline phases were identified using the ICDD database.

Temperature-programmed desorption of ammonia (NH_3-TPD) was conducted to investigate the acidic properties of the catalysts. Prior to the analyses, 200 mg of the catalyst was treated at 500 °C for 1 h in He to remove adsorbed water and organic species. After saturating with a 15 vol% NH_3/He mixture gas at 150 °C for 30 min, the catalysts were degassed with He for 1.2 h. NH_3 was then desorbed in the temperature range of 150–500 °C at a heating rate of 5 °C/min under a flow of He at 50 mL min^{-1}. The desorbed NH_3 was monitored by thermal conductivity detector (TCD) signals (Micromeritics, AutoChemII 2920).

Temperature-programmed desorption of isopropyl amine (IPA-TPD) was performed to determine the Brønsted acidity of the catalysts. The same pretreatment procedures as those used in the NH_3-TPD experiments were used, except that 2 vol% IPA/He was used for saturation. Then, IPA was desorbed in the temperature range of 100–500 °C at a heating rate of 10 °C/min under a flow of He at 50 mL min^{-1}. The Brønsted acidity was determined by decomposition of IPA to propylene and NH_3 through a Hoffman-type elimination reaction [38,39].

Thermogravimetric analysis (TGA) was performed on a SDT Q600 instrument (TA Instruments) with 30–40 mg of each sample in the temperature range of 30–900 °C at a heating rate of 5 °C min^{-1} under a constant air flow at 100 mL min^{-1}. The amount of coke and its combustion heat were obtained from the total weight loss and integration of the heat flow.

Diffuse reflectance infrared Fourier transform (DRIFT) spectroscopy was carried out using a commercial in situ reaction cell (Harricks, HV-DR2). The spectra were collected using a Nicolet Nexus 4700 spectrometer (Thermo) equipped with a mercury-cadmium-telluride-B detector. Thirty milligrams of the spent Mo/H-ZSM-5 catalyst collected after the reaction was carefully loaded in the sample holder locating in the middle of the DRIFT cell. After pre-treatment at 200 °C for 3 h with flowing He to remove adsorbed water, the cell was cooled to room temperature, and the background spectrum was collected while flowing the target gas (i.e., 10% O_2 balanced with He for regeneration with O_2 and 10% H_2 balanced with He for regeneration with H_2) at the desired temperature. Regeneration of the spent catalyst was investigated at 400, 450, 500, and 550 °C for 30 min, and the IR spectra were collected after regeneration at each temperature.

Raman spectroscopy was performed for coke analysis of the spent Mo/H-ZSM-5 catalysts by a LabRAM HR Evolution instrument (Horiba, Ltd.) under ambient conditions. For the analysis, a 514 nm laser source was used for excitation.

Temperature-programmed reduction (TPR) was conducted with 100 mg of the spent samples in the temperature range of 50–900 °C at a heating rate of 10 °C min^{-1} under a constant flow of 5% H_2/He at 50 mL min^{-1}. The spent catalysts were purged with He at 300 °C for 1 h prior to the TPR experiments. A water trap containing a mixture of dry ice and acetone was used to remove the moisture in the effluent before the TCD analysis. The TCD signals of the effluent were recorded on an AutoChemII 2920 unit (Micromeritics).

Transmission electron microscopy (TEM) was conducted to identify the morphologies of the Mo/H-ZSM-5 catalysts after the 5 cycle MDA reactions including oxidative regeneration. The TEM images were obtained with a FEG S/TEM instrument (Talos F200S) at 200 kV.

The thermodynamic equilibrium under coke regenerating condition was calculated by the Gibbs free energy minimization method using HSC chemistry software (Qutotec). The amount of coke deposition used was that of 5Mo/H-ZSM-5 catalyst in the TGA data.

X-ray absorption spectroscopy (XAS) was conducted using beamline 8C (Nano XAFS) at the Pohang Accelerator Laboratory (PAL). A Si (111) double crystal was used to generate a monochromatic X-ray beam. The spectroscopic data were collected in transmittance mode with an electron energy of 3.0 GeV and a ring current of 70–100 mA. To calibrate

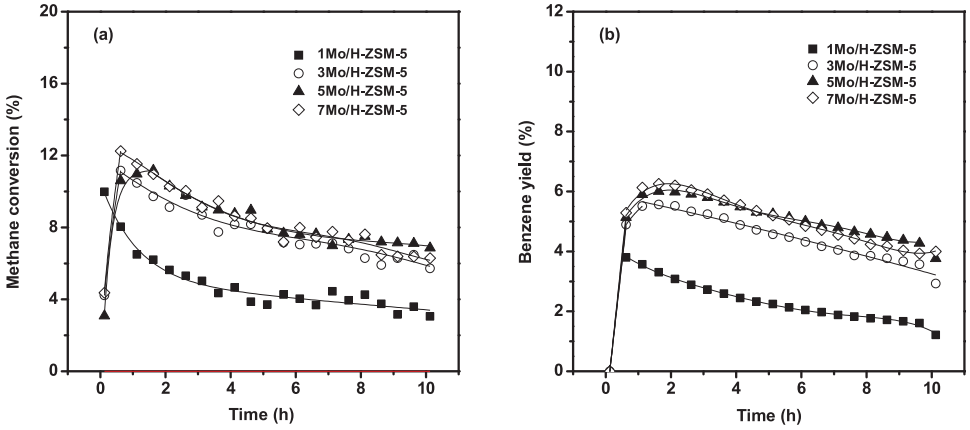

Fig. 1. Methane conversion and benzene yield with time on stream in the MDA reaction over XMo/H-ZSM-5 (X = 1, 3, 5, and 7) catalysts.

the samples, Mo foil was used as the reference. For the analysis, a mixture of N_2/Ar gas in the ionization chambers was adjusted to optimize the intensities of I_0 and I. XANES and EXAFS data were analyzed using the Athena software package [40]. The energy scale was calibrated from the edge energy position of Mo foil (20 keV). The k^3-weighted EXAFS was Fourier transformed in the range of 0–8 Å.

2.3. Methane dehydroaromatization (MDA)

Methane dehydroaromatization (MDA) was carried out in a fixed-bed quartz reactor at atmospheric pressure at 700 °C. The total weight hourly space velocity (WHSV) was fixed at 1500 mL g_{cat}^{-1} h^{-1}. The reactor was 39 cm long and had an inner diameter of 8.46 mm. A uniform temperature profile along the catalyst bed was achieved by using three different heating zones with an aluminum heating block inserted into the void space between the furnace and the tubular reactor. The temperature was monitored by three different K-type thermocouples directly contacting the aluminum block. For the catalytic activity measurements, the prepared catalysts were pelletized and sieved to a uniform diameter of 425–850 μm mesh size before the reaction. The sieved catalysts (0.4 g) were placed in the center of the quartz reactor and supported by 5 mm of quartz wool. To prevent condensation of the aromatic products, all lines from the reactor to the online gas chromatograph were heated to 220 °C. Prior to each reaction, the catalyst was purged by 30 mL min^{-1} of He by increasing the temperature to 700 °C at a rate of 10 °C min^{-1}, which was maintained for 1 h. After pretreatment, the mixed gas containing 90% methane and 10% Ar was fed into the reactor using mass flow controllers (1179A, MKS Instruments). For quantitative analysis, Ar was used as an internal standard. The regeneration was conducted at atmospheric pressure under the mixed gas containing 10% oxygen or hydrogen and 90% helium. During the regeneration, the total WHSV was fixed at 7500 mL g_{cat}^{-1} h^{-1}.

Gas analysis was conducted using an online gas chromatograph (YL 6500GC, Younglin) equipped with three blocks of detectors composed of one thermal conductivity detector (TCD) and two flame ionization detectors (FID). The amount of H_2, CH_4, Ar, CO, CO_2, and C2 components were determined by TCD with a ShinCarbon ST instrument (Restek Corp., Catalog No. 80486-800). Both the injection port and the detector were held at 200 °C. The column flow rate of the He carrier gas was 20 mL min^{-1}. C1–C4 hydrocarbons and benzene were analyzed using a FID with an Alumina BOND/Na_2SO_4 column (Restek Corp., Catalog No. 19756). The injection port and the detector were held at 200 and 250 °C, respectively. The column flow rate of the He carrier gas was 9 mL min^{-1}. C_{6+} compounds including benzene and naphthalene were separated on an Rtx-VMS column (Restek Corp., Catalog No. 49915) and detected on an additional FID. The injection port and the detector were held at 200 and 250 °C, respectively. The column flow rate of the He carrier gas was 0.5 mL min^{-1}. The following GC oven temperature regime was used: temperature held at 50 °C for 6 min, increased to 200 °C at 15 °C/min, and held at 200 °C for 8 min.

The methane conversion was calculated as moles of methane reacted per moles of methane fed into the system. The yield was calculated by carbon moles of product divided by carbon moles of methane fed into the system. The methane consumption rate was calculated as moles of converted methane divided by weight of catalyst per hour. The product formation rate was calculated as carbon moles of products divided by weight of catalyst per hour.

2.4. Computational details

The energetics of the coke oxidation and hydrogenation were compared along their respective reaction coordinates using density functional theory (DFT) with a plane-wave basis set, as implemented in the Vienna Ab-Initio Simulation Package (VASP) [41,42]. The revised Perdew–Burke–Ernzerhof (rPBE) [43] exchange-correlation functional in the generalized gradient approximation was used. The kinetic energy cutoff was set to 450 eV, and van der Waals interactions were considered using vdW-DF [44–47]. A Monkhorst–Pack k-points mesh grid of 1 × 1 × 1 was used throughout the calculations for Brillouin zone sampling. The Gibbs free energy of the gas-phase species was calculated based on the ideal gas limit, in which the vibrational, translational, and rotational degrees of freedom were considered, whereas that of the adsorbed species was calculated based on the harmonic limit, for which only the vibrational degrees of freedom were considered [48].

A periodic 96T model was used to simulate the ZSM-5 structure. A Mo_2C, MoO_3 or Mo cluster was placed at the intersection of straight and sinusoidal channels of ZSM-5. The calculated structures of H-ZSM-5, Mo_2C/H-ZSM-5, MoO_3/H-ZSM-5, and Mo/H-ZSM-5 are shown in Fig. S15.

3. Results and discussion

3.1. Methane dehydroaromatization over the Mo/H-ZSM-5 catalysts

Fig. 1 shows methane conversion and benzene yield with time during the MDA reaction at 700 °C over the Mo/H-ZSM-5 catalysts. All the catalysts have a maximum methane conversion at 1 h and benzene yield at 1.5 h of reaction time. This is because the initial activation process includes Mo_2C formation through MoO_3 carburization [49], which subsequently undergoes slow deactivation during the reaction. It appears that a 1 wt% loading of Mo in the Mo/H-ZSM-5 catalyst is insufficient for methane activation in the MDA reaction (Tables S1 and S2). In contrast, Mo/H-ZSM-5 catalysts with Mo loadings of 3, 5, and 7 wt% exhibited similar methane conversions and benzene yields. Among them, the 5Mo/H-ZSM-5 catalyst performed somewhat better

than the other catalysts until the end of the reaction. This is probably due to the high accessibility of Mo_2C and Brønsted acid sites in the microchannels of H-ZSM-5 (Figs. S1, S2, and Table S3). 5 wt% Mo is the optimal for H-ZSM-5 (SiO_2/Al_2O_3 = 30) to maintain high Mo dispersion (Table S3 and Fig. S3(a)). The benzene yield of the catalysts obtained after 10 h decreased in the order of 5Mo/H-ZSM-5 > 7Mo/H-ZSM-5 > 3Mo/H-ZSM-5 > 1Mo/H-ZSM-5. It is known that molybdenum oxide is dispersed in the form of MoO_4^{2-} by anchoring on the Brønsted acid sites [35,50–53]. Therefore, the low ratio of Brønsted to Lewis acid sites on the 5Mo/H-ZSM-5 catalyst (Fig. S4 and Table S3) is indicative of high Mo dispersion and high Mo proximity with Brønsted acid sites.

The catalytic performance of XMo/H-ZSM-5 catalyst was compared in terms of methane conversion, benzene yield, and normalized reaction rate, as shown in Table S4. The normalized reaction rate was calculated based on the moles of Mo on H-ZSM-5. The initial catalytic performances at reaction time of 1.5 h were also compared with those at 10 h. The normalized reaction rate was decreased with increasing Mo content, indicating that Mo dispersion of catalyst decreased with increasing Mo content. This explains why 7Mo/H-ZSM-5 retained lower methane conversion than 5Mo/H-ZSM-5 catalyst despite higher Mo content. The benzene yield was inversely proportional to the normalized reaction rate, which is likely due to a decrease in Brønsted acid sites as the Mo content increased (Table S3). It is noteworthy that the normalized reaction rate was drastically decreased after 10 h-reaction due to coke formation.

The methane conversion decreased with time on stream over all the tested catalysts (Fig. 1). To compare the differences in activity, the formation rate of major products was plotted as a function of methane consumption rate, as shown in Figs. 2 and 3. It is noteworthy that the formation rates of ethylene (Fig. 2(b)) and propylene (Fig. 2(c)) increased with decreasing methane consumption rate, whereas those of benzene (Fig. 3(a)) and naphthalene (Fig. 3(b)) decreased. Therefore, it is inferred that deactivation of the zeolite acid sites likely precedes deactivation of the Mo_2C sites.

According to the literature [54], ethane formation rate should be decreased as the methane consumption rate decreases due to the decrease of the benzene formation reaction rate ($4C_2H_4 \rightarrow C_6H_6 + C_2H_6 + 2H_2$). However, except for the 1Mo/H-ZSM-5 catalyst, the ethane formation rate (Fig. 2(a)) increased as the methane consumption rate decreased. This may be because the ethylene hydrogenation reaction at the Mo carbide sites ($C_2H_4 + H_2 \rightarrow C_2H_6$) increased as the ethylene formation rate increased.

The largest decrease in the benzene formation rate (Fig. 3(a)) as the methane consumption rate decreased occurred for the 1Mo/H-ZSM-5 catalyst. However, this catalyst, which possesses the highest acid site/Mo_2C site ratio, exhibited the highest naphthalene formation rates at similar methane consumption rates (Fig. 3(b)). This implies that a high acid site/Mo_2C site ratio induces naphthalene formation, leading to the formation of coke. According to the proposed reaction pathway [54], benzene can be converted to naphthalene through toluene and alkyl aromatics at the zeolite acid sites. Therefore, the high naphthalene formation rate in the 1Mo/H-ZSM-5 catalyst (Fig. 3(b)) and the high alkyl aromatic formation rate in the 3Mo/H-ZSM-5 catalyst (Fig. 3(d)) indicate that an excessively high acid site/Mo_2C site ratio is unfavorable for benzene production but favorable for alkyl aromatic and naphthalene formation.

The MDA reaction results are in good agreement of the mechanism proposed on the basis of the previous literatures (Fig. 4) [1,54–58]. This pathway involves a series of metal- and acid-catalyzed reactions to produce olefins, paraffins, aromatics, and cokes. The tested Mo/H-ZSM-5 catalysts convert methane through a bifunctional reaction pathway in which the Mo_2C sites produce ethylene and propylene and the Brønsted acid sites further convert these olefins to produce benzene [53,59,60]. The ethylene may undergo hydrogenation reaction to form ethane in the presence of Mo carbide sites on H-ZSM-5. The benzene undergoes further reaction to produce the corresponding (alkyl)-aromatics with a high carbon number. Undesirable coke formation can take place from both olefins and aromatics. According to the hydrocarbon-pool mechanism, polyaromatic hydrocarbon also can react with C_2H_x to form benzene and this was also reflected in the mechanism (Fig. 4) [61]. The Mo_2C sites may have a lower rate of coke formation than the Brønsted acid sites. It is therefore important to minimize the surface concentration of isolated acid sites to increase catalytic stability. The localization of Mo_2C sites as well as that of Brønsted acid sites in zeolite channels is probably important because it determines the catalytic properties. Therefore, it is inferred that formation of highly dispersed MoO_3 species associated with the Brønsted acid sites is key for the MDA [62,63]. Likewise, the best catalytic performance of 5Mo/H-ZSM-5 catalyst (Fig. 1) can be explained by its reduced isolated acid sites with high Mo dispersion.

3.2. Characterization of the spent Mo/H-ZSM-5 catalysts

Fig. 5 shows the TG/DTG/DSC profiles of spent Mo/H-ZSM-5 catalysts after 10 h of the MDA reaction. According to the literature, the slight weight increase below 400 °C is caused by oxidation of molybdenum carbide species ($Mo_2C + 4O_2 \rightarrow 2MoO_3 + CO_2$) [4]. From the TG/DTG analysis, the type of coke was distinguished relative to the weight loss temperature in the range of 400–500 °C and 500–650 °C; L–T coke decomposes at low temperature, whereas H–T coke decomposes at high temperature. The Raman spectrum of the spent 5Mo/H-ZSM-5 catalyst regenerated under O_2 conditions at 450 °C (Fig. S5) exhibited peaks only for poly-aromatic coke at 1354 and 1605 cm^{-1}. This demonstrates that H–T coke is mainly composed of poly-aromatic coke, which is consistent with previous reports [58,64]. Therefore, the sharp peak at 450 °C (L–T coke) is mainly attributed to graphite coke

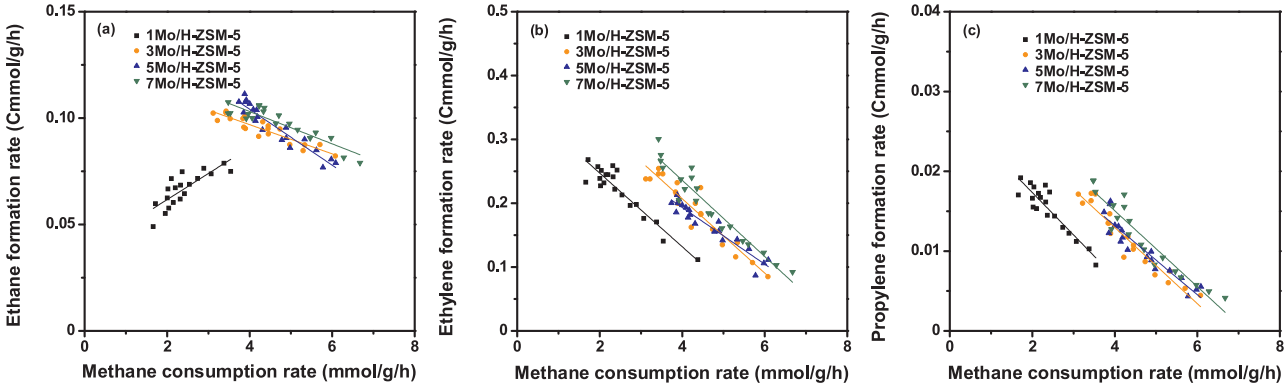

Fig. 2. The formation rate of (a) ethane, (b) ethylene, and (c) propylene over XMo/H-ZSM-5 (X = 1, 3, 5, and 7) catalysts, plotted as a function of methane consumption rate.

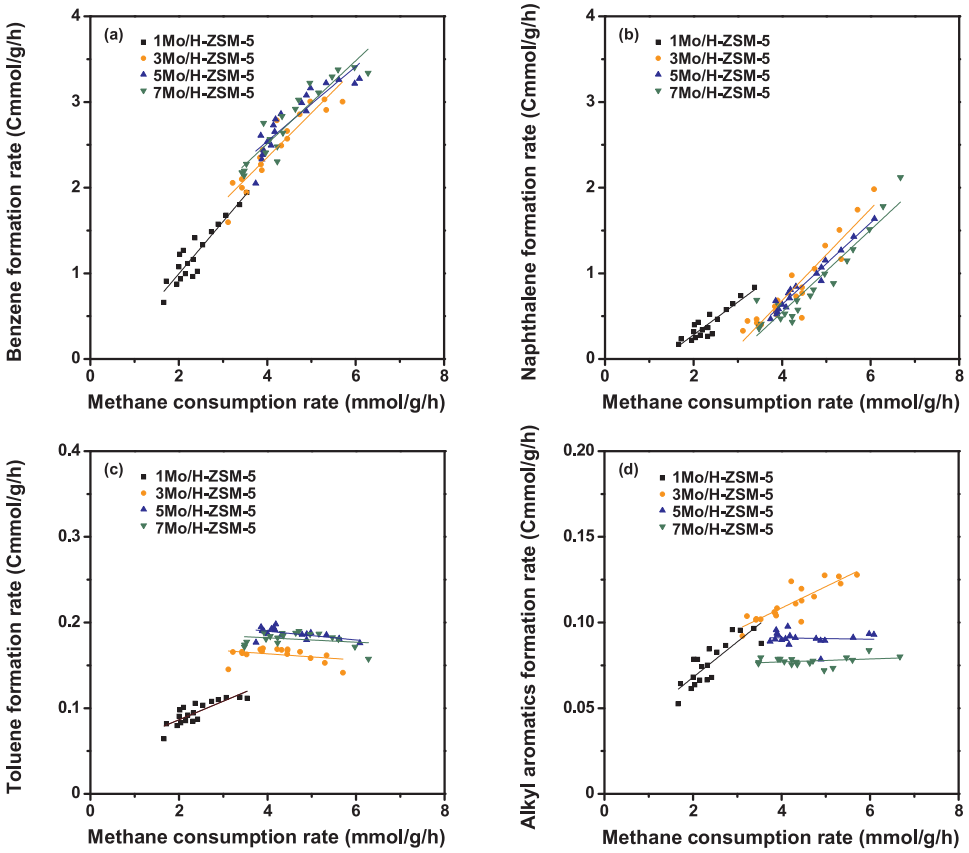

Fig. 3. The formation rate of (a) benzene, (b) naphthalene, (c) toluene, and (d) alkyl aromatics over XMo/H-ZSM-5 (X = 1, 3, 5, and 7) catalysts, plotted as a function of methane consumption rate.

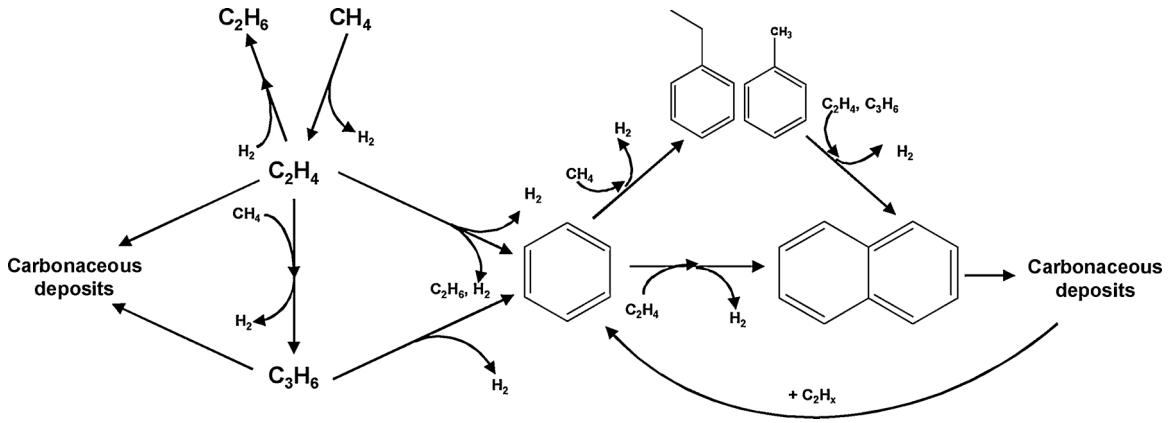

Fig. 4. The mechanism of methane dehydroaromatization over Mo/H-ZSM-5 catalyst.

near the Mo sites, while the tailing peak at higher temperature (H–T coke) can be attributed to poly-aromatic coke at the acid sites [55]. As shown in the DSC profiles of the used catalysts (Fig. 5(c)), the L–T coke retained a relatively high heat flow compared with the H–T coke. This is probably because the L–T coke was mostly oxidized by complete catalytic combustion ($10C + 10O_2 \rightarrow 10CO_2$, $\Delta H_{450\ ^\circ C} = -941.7$ kcal), whereas the H–T coke was oxidized incompletely ($C_{10}H_8 + 7O_2 = 10CO + 4H_2O$, $\Delta H_{535\ ^\circ C} = -532.0$ kcal). Further, the 5Mo/H-ZSM-5 and 7Mo/H-ZSM-5 catalysts retained a decomposition peak at higher temperatures (> 800 °C), which is attributed to the sublimation of MoO_3 [27] (Fig. 5(b)). This result indicates that oxidative regeneration at high temperature (> 800 °C) is vulnerable to MoO_3 sublimation. The amount of coke was calculated from each deconvoluted area in the DTG profiles (Table 1). It was observed that the amount of H–T coke decreased with increasing Mo loading. This is probably because the formation rate of poly-aromatic coke decreased as the Mo site/Brønsted acid site ratio increased for the Mo/H-ZSM-5 catalysts during the reaction. On the other hand, the amount of L–T coke decreased in the order of 3Mo/H-ZSM-5 > 5Mo/H-ZSM-5 > 7Mo/H-ZSM-5 > 1Mo/H-ZSM-5. The lowest L–T coke deposition on 1Mo/H-ZSM-5 catalyst might be due to its deficient Mo sites for methane conversion. While, low amount of L–T coke in 5Mo/H-ZSM-5 and 7Mo/H-ZSM-5 might be due to their high Mo site/Brønsted acid site ratio. Despite the larger amount of poly-aromatic coke, 5Mo/H-ZSM-5 catalyst exhibited higher benzene yield compared to 7Mo/H-ZSM-5 catalyst. This indicates that benzene formation by hydrocarbon-pool mechanism was favorable in 5Mo/H-ZSM-5 catalyst [61].

Raman spectroscopy was performed to determine the type of coke

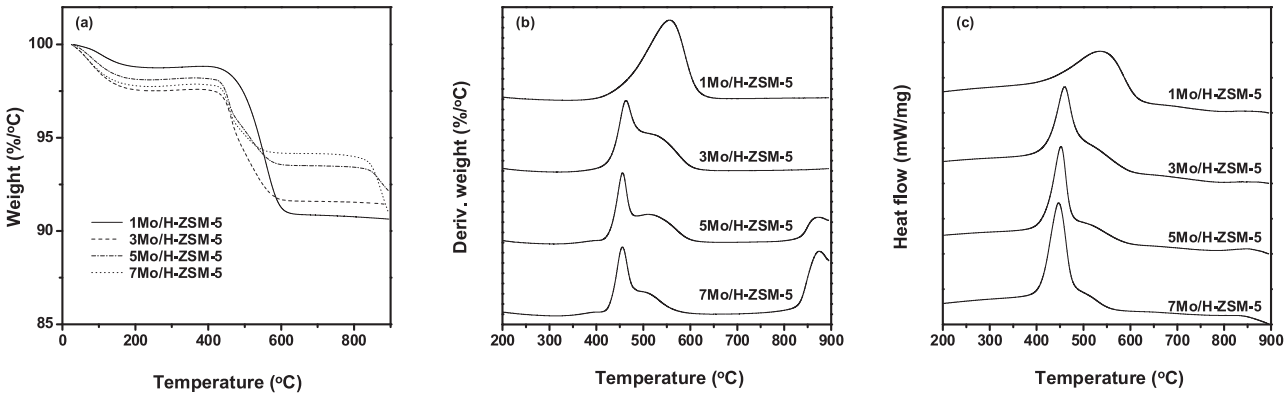

Fig. 5. (a) TG, (b) DTG, and (c) DSC profiles of used XMo/H-ZSM-5 (X = 1, 3, 5, and 7) catalysts obtained after a 10 h-MDA reaction.

Table 1
Amount of carbon deposition in the XMo/H-ZSM-5 catalysts after 10 h-reaction.

Catalyst	Carbon deposition (wt%)[a]			
	400–500 °C	500–650 °C	L–T coke/H–T coke ratio	Total
1Mo/H-ZSM-5	1.30	6.32	0.21	7.91
3Mo/H-ZSM-5	2.45	3.26	0.75	5.95
5Mo/H-ZSM-5	1.89	2.51	0.75	4.65
7Mo/H-ZSM-5	1.82	1.49	1.22	3.65

[a] Calculated from deconvoluted peak area of DTG profiles in Fig. 5(b).

present in the spent catalysts (Fig. S6). For this purpose, the Raman spectra were deconvoluted into five Lorentz peaks based on previous literature [65,66]. The shoulder band at 1200 cm^{-1} (I_{C-H}) is attributed to C—H vibrations and the G-band (I_G, 1550–1600 cm^{-1}) is attributed to the stretching mode of sp^2-hybridized carbon bonds of ordered graphitic carbon. The D-band of the aromatic coke was subdivided into three types: the D1 band at 1350 cm^{-1} is attributed to the vibrations of disordered carbon; the D2 band at 1600–1610 cm^{-1} is attributed to the vibrations of disordered aromatic structures; and the D3 band at 1450–1510 cm^{-1} is attributed to the vibrations of defects of the carbon structure. The characteristic fraction of the deconvoluted areas of the bands and peak position of the D2 band are summarized in Table 2. It is noteworthy that the integrated area of the I_G/I_{D2} ratio increased with increasing molybdenum loading. As with the Raman results (Fig. S5), it was confirmed that L–T coke is mainly composed of graphite-like coke, whereas H–T coke is mainly composed of poly-aromatic coke, which is in agreement with previous research [58].

Fig. S7 shows the TPR profiles of the spent Mo/H-ZSM-5 catalysts after 10 h of use. Similar to the TG/DTG results, two reduction peak for coke hydrogenation (i.e., L–T and H–T) were observed. It is noteworthy that the coke hydrogenation temperature under reductive conditions was higher than coke oxidation temperature under oxidative conditions. Indeed, temperatures of at least 700 °C is required for coke hydrogenation. Because Mo_2C sites catalyzes hydrogenation or hydrogenolysis of naphthalene, L–T reduction peak might be attributed to hydrogenation of coke near Mo sites [67]. While, H–T coke might be attributed to hydrogenation of coke near acid sites. Interestingly, sublimation of molybdenum was not observed in this case due to the low sublimation property of reduced Mo species (Mo_2C or Mo^0).

3.3. Oxidative regeneration of the Mo/H-ZSM-5 catalysts

The MDA reaction was conducted at atmospheric pressure and 700 °C, including regeneration in 10% O_2/He at temperatures in the range of 450–850 °C. The methane conversions and benzene yields in a 5-cycle reaction at various regeneration temperatures are displayed in Fig. 6. Among these temperatures, 450 °C proved to be the most effective and the benzene yield was slightly increased after regeneration. As shown in the TG/DTG results in Fig. 7, regeneration at 450 °C can selectively remove L–T coke. In the IPA-TPD results of the regenerated catalysts (Fig. S8 and Table S5), it was observed that Brønsted acid sites were quite restored under oxidative condition at 450 °C. According to the literature, this is attributed to the removal of Mo-associated coke on the external zeolite surface blocking zeolite channels [55,56]. Nevertheless, oxidative regeneration at 450 °C left some coke on Brønsted acid sites which doesn't affect the catalytic activity. This indicates that isolated acid sites, which is not regenerated, are not involved in benzene formation but rather are involved in naphthalene formation. Considering the mechanistic study in Section 3.1, regeneration of acid sites near Mo sites is sufficient to recover catalytic activity. On the other hand, oxidative regeneration at 550 °C efficiently regenerated Brønsted acid sites of catalyst by oxidizing H–T coke. Although regeneration at 550 °C efficiently removes both L–T coke and H–T coke, catalytic deactivation in the 1-cycle reaction gradually increased over 5 cycles. This is probably because regeneration at 550 °C is disadvantageous in terms of MoO_3 sintering, which might increase amount of isolated acid sites. In the high–temperature regeneration tests (i.e., 700 and 850 °C), the catalyst experienced severe deactivation for methane conversion and benzene yield. Moreover, the selectivity for ethylene rapidly increased as the recycle-reaction progressed (Fig. S9), indicating that the Brønsted acid sites were irreversibly deactivated during regeneration. This may occur because not only is MoO_3 susceptible to sublimation under oxidative conditions at high temperatures, but the Brønsted acidity of the zeolite is also vulnerable [68].

N_2 adsorption-desorption measurements were conducted to determine the textural properties of 5Mo/H-ZSM-5 catalyst after a 5

Table 2
Characteristic fraction of deconvoluted area of bands assigned in the Raman spectra of XMo/H-ZSM-5 catalysts after a 10 h-reaction.

Catalyst	I_{C-H} (%)[a]	I_{D1} (%)[a]	I_{D3} (%)[a]	I_G (%)[a]	I_{D2} (%)[a]	P_{D2} (cm^{-1})	I_G/I_{D2}
1Mo/H-ZSM-5	12.4	39.7	10.5	13.3	24.1	1612	0.55
3Mo/H-ZSM-5	7.6	47.6	10.2	15.8	18.8	1611	0.84
5Mo/H-ZSM-5	6.6	46.3	10.9	16.6	19.6	1611	0.85
7Mo/H-ZSM-5	6.2	48.5	13.3	17.1	14.8	1613	1.16

[a] Calculated from deconvoluted peak area of Raman spectra in Fig. S6.

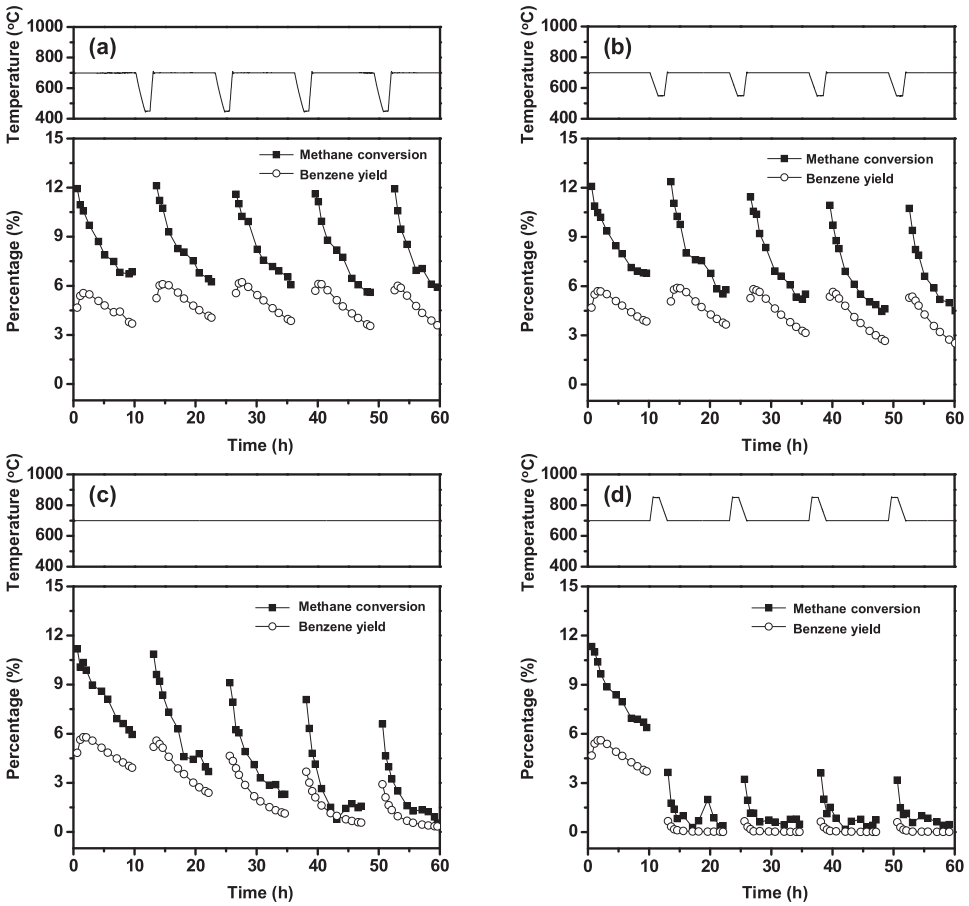

Fig. 6. Methane conversion and benzene yield in the 5 recycle-MDA reaction including oxidative regeneration at (a) 450 °C, (b) 550 °C, (c) 700 °C, and (d) 850 °C over 5Mo/H-ZSM-5 catalyst.

recycle MDA reaction as summarized in Table S6. The surface area and pore volume of the 5Mo/H-ZSM-5 catalyst (Table S2) decreased after a 5 recycle-MDA reaction including oxidative regeneration. This might be due to coke deposition in zeolite pores and thermal degradation during the MDA reaction at 700 °C. In particular, the decrease of the micro pore volume might be the main cause of deactivation by inducing the loss of Brønsted acid sites in the inner pores [69]. Also, the drastic decrease of surface area and pore volume was observed in oxidative regeneration at 850 °C. As can be seen from the decrease of crystallinity in XRD (Fig. S10(a)), it is inferred that zeolite framework collapsed through the formation of aluminum molybdate at high temperature [27].

TGA analysis was conducted to investigate the effect of oxidative regeneration on coke formation, as shown in Fig. 7. The amount of L–T and H–T coke deposition was calculated from the deconvoluted areas of the DTG profiles (Table 3). As mentioned previously, coke desorbed at low temperature (400–500 °C, L–T coke) indicates coke deposited near Mo sites, whereas coke desorbed at high temperature (500–650 °C, H–T coke) indicates poly-aromatic coke on isolated acid sites. As expected from the TG/DTG results, the '5 Recycle (O_2, 450 °C)' sample with the best regenerability retained the largest amount of H–T coke among the catalysts. This implies that poly-aromatic coke on the catalyst was not

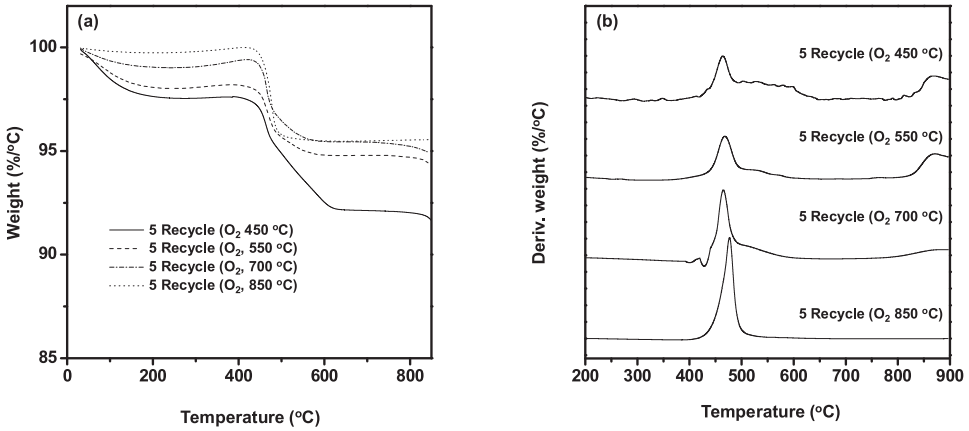

Fig. 7. (a) TG and (b) DTG profiles of used 5Mo/H-ZSM-5 catalysts obtained after a 5 recycle-MDA reaction including oxidative regeneration at 450 °C, 550 °C, 700 °C, and 850 °C.

Table 3
Amount of carbon deposition in the 5Mo/H-ZSM-5 catalysts after a 5 cycle-MDA reaction including oxidative regeneration.

Catalyst	Carbon deposition (wt%)[a]			
	400–500 °C	500–650 °C	L–T coke/H–T coke ratio	Total
5 Recycle (O_2 450 °C)	2.14	3.02	0.71	5.16
5 Recycle (O_2 550 °C)	2.22	1.19	1.86	3.41
5 Recycle (O_2 700 °C)	2.52	1.19	2.12	3.71
5 Recycle (O_2 850 °C)	5.56	–	–	5.56

[a] Calculated from deconvoluted peak area of DTG profiles in Fig. 7(b).

completely removed under oxidative regeneration at 450 °C but instead accumulated as the reaction cycle progressed. This further confirmed that polyaromatic coke deposited on isolated acid sites are not important for benzene formation; regeneration of Brønsted acid sites near Mo sites is crucial for regeneration. In the same context, the amount of H–T coke decreased with increasing regeneration temperature. In particular, the '5 Recycle (O_2, 850 °C)' sample retained only L–T coke, unlike the other samples. Therefore, it appears that oxidative regeneration at 850 °C induces not only severe sublimation of MoO_3 but also loss of Brønsted acidity.

Fig. S11 shows the Raman spectrum of the 5Mo/H-ZSM-5 catalyst after a 5 O_2 recycle-reaction. As in Table 4, the spectrum was deconvoluted into five peaks. The integrated area of the G-band to D2-band ratio increased with increasing regeneration temperature, which is consistent with the trend of the L–T coke/H–T coke ratio observed in the TGA analysis. Interestingly, the peak position of poly-aromatic coke shifted to a lower value compared with the Mo/H-ZSM-5 catalyst after a 1-cycle reaction (Fig. S6). This reveals that deposited aromatic carbon became condensed over the 5-recycle reaction. Nevertheless, the Mo/H-ZSM-5 catalyst regenerated with O_2 at 450 °C did not decrease the benzene yield over 5 cycles (Fig. S9). In the case of the '5 Recycle (O_2, 850 °C)' sample, a small peak area for aromatic compounds (I_{D2}) was observed, which is attributed to its poor catalytic activity for aromatization after regeneration.

In order to investigate the Mo morphology of the catalyst after the 5-cycle MDA reaction, TEM analysis was conducted (Fig. 8). In the 5Mo/H-ZSM-5 catalyst with oxidative regeneration at 450 °C (Fig. 8(a)), small and large Mo_2C particles can be distinguished. Since Mo_2C is more likely to be aggregated than MoO_3, large Mo_2C particles may be derived from molybdenum oxides on the external surface of the zeolite. By comparison, small Mo_2C particles may be derived from isolated MoO_3 species closely interacting with Brønsted acid sites [49]. The Mo_2C on the external surface of the zeolite not only reduces Mo_2C dispersion by sintering but also blocks the micropores by coke formation, which is the main cause of deactivation. It was reported that initial MoO_3 anchored on Al sites of the zeolite framework induces higher catalytic activity by converting stable Mo carbides to those that anchored on Si sites of external surface [62]. Fig. 8(b)–(d) show the TEM images of the '5 Recycle (O_2, 550 °C)', '5 Recycle (O_2, 700 °C)', and '5 Recycle (O_2, 850 °C)' samples, respectively. Interestingly, the ratio of large Mo_2C on the zeolite's external surface increased with increasing regeneration temperature. Therefore, MoO_3 is likely to be predominantly formed on the external surface, thereby inducing the formation of large Mo_2C particles at high temperature regeneration [49,52]. In addition, the stability of the catalyst decreased irreversibly with the reaction cycle. In particular, '5 Recycle (O_2, 850 °C)' retained some voids in the zeolite framework with a decreased number of Mo_2C particles. This may be caused by damage to the zeolite framework by the formation of aluminum molybdate at high regeneration temperatures [27]. The MoO_3 sublimation and collapse of the framework also induced an irreversible decrease of the number of Mo and Brønsted acid sites, resulting in a drastic deactivation after regeneration. Consequently, it was confirmed that regeneration at 450 °C is an optimal temperature for maintaining the zeolite framework and high Mo_2C dispersion.

3.4. Reductive regeneration of the Mo/H-ZSM-5 catalysts

In oxidative regeneration, the optimum temperature (450 °C) was significantly lower than the reaction temperature (700 °C). For this reason, cyclic reductive regeneration is probably more suitable for continuous reaction system and has been attempted [35,70]. The MDA reaction with regeneration under an atmosphere of 10% H_2/He in the temperature range of 450–850 °C was conducted, as shown in Fig. 9. It was observed that regeneration temperatures of 450 °C (Fig. 9(a)) and 550 °C (Fig. 9(b)) showed no effect in terms of either methane conversion or benzene yield. Therefore, regeneration temperatures below 700 °C are not effective to remove Mo-associated coke and acid site-associated poly-aromatic coke under H_2/He conditions. For regeneration at 700 °C (Fig. 9(c)), the conversion of methane and yield for benzene slightly increased after regeneration. Although coke hydrogenation occurred at 700 °C (Fig. S7), the catalytic activity barely recovered. This indicates that coke is partially hydrogenated at 700 °C and remained as a hydrocarbon on Mo_2C. Regeneration at 850 °C exhibited much better catalytic performance than that at 700 °C. In particular, the first regeneration process restored most of the catalysts' reactivity in terms of benzene yield, since most of coke was removed by hydrogenation. Additionally, regeneration under 10% H_2/He was much more successful than that under 10% O_2/He at 850 °C (Fig. 6(d)). This is because the thermal stability of Mo species (Mo_2C or Mo°) is much higher than MoO_3 at 850 °C due to its low sublimation property [71]. However, methane conversion decreased continuously as the reaction cycle progressed, even at high regeneration temperature. This is because partially hydrogenated Mo_2C sites experienced sintering during the regeneration process due to weak interactions between Mo_2C and H-ZSM-5; a decrease of benzene selectivity was also observed, demonstrating that the number of acid sites adjacent to Mo_2C decreased by Mo sintering (Fig. S12). Consequently, it was found that temperatures of at least 850 °C are required for reductive regeneration and that this type of regeneration is inefficient compared with oxidative regeneration due to the Mo_2C sintering at high regeneration temperature.

The BET result shows that surface area and pore volume of the 5Mo/H-ZSM-5 catalyst drastically decreased after a 5 recycle-MDA reaction including reductive regeneration (Table S6). Particularly, decrease of zeolite micro pore indicates that coke confined in micropores was not regenerated after the reductive regeneration. On the other hand,

Table 4
Characteristic fraction of deconvoluted area of bands assigned in the Raman spectra of 5Mo/H-ZSM-5 catalysts after a 5 cycle-MDA reaction including oxidative regeneration.

Catalyst	$I_{C\text{-}H}$ (%)[a]	I_{D1} (%)[a]	I_{D3} (%)[a]	I_G (%)[a]	I_{D2} (%)[a]	P_{D2} (cm^{-1})	I_G/I_{D2}
5 Recycle (O_2 450 °C)	5.2	51.9	11.8	14.1	17.0	1604	0.83
5 Recycle (O_2 550 °C)	5.1	50.5	13.4	19.5	11.5	1608	1.69
5 Recycle (O_2 700 °C)	4.8	62.4	5.0	17.4	10.4	1604	1.68
5 Recycle (O_2 850 °C)	5.9	60.5	5.5	21.1	7.1	1605	2.96

[a] Calculated from deconvoluted peak area of Raman spectra in Fig. S11.

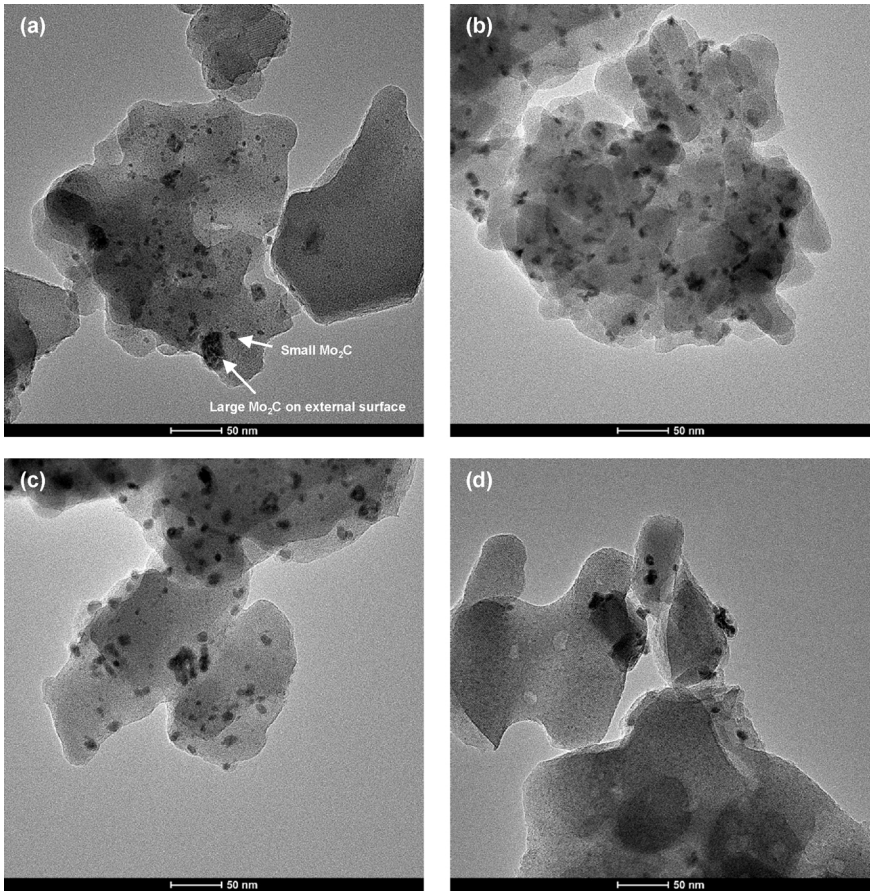

Fig. 8. TEM images of used 5Mo/H-ZSM-5 catalysts obtained after a 5 recycle-MDA reaction including oxidative regeneration at (a) 450 °C, (b) 550 °C, (c) 700 °C, and (d) 850 °C.

crystallinity of zeolite MFI structure was well maintained after the reaction (Fig. S10(b)).

Fig. 10 shows the TG/DTG profiles of Mo/H-ZSM-5 after the 5-recycle test with H_2 regeneration at various temperatures (450, 550, 700, and 850 °C). The amount of carbon deposition calculated from the TG/DTG profile is summarized in Table 5. It was observed that the amount of coke deposition after H_2 regeneration was larger than that after O_2 regeneration. Moreover, the amount of coke did not decrease even after the 5-cycle reaction, including regeneration at 700 °C and 850 °C at which coke hydrogenation can occur. This is because coke hydrogenation on Mo_2C is more disadvantageous than coke oxidation on MoO_3 in terms of dispersion and coke removal efficiency. Similar results were obtained from DRIFT spectroscopy (Fig. S13). Here, it was observed that the intensity decrease at 1622 cm^{-1}, which is associated with the vibration of complex aromatics, was more pronounced in oxidative (Fig. S13(b)) rather than in reductive (Fig. S13(a)) regeneration [65,72], demonstrating that coke hydrogenation is less efficient than oxidation for regeneration. This was further confirmed by IPA-TPD profiles of 5Mo/H-ZSM-5 catalyst after a 5 recycle-reaction including oxidative regeneration and reductive regeneration (Fig. S8 and Table S5). The samples were reoxidized or rehydrogenated before the analysis. The Brønsted acid sites of catalyst was successfully restored in oxidative regeneration at 450 °C and 550 °C. On the other hand, reductive regeneration at 450 °C and 550 °C didn't restore the Brønsted acid sites of catalyst indicating that coke on the acid sites were not hydrogenated below 550 °C. The equilibrium composition under the condition of regenerating 5Mo/H-ZSM-5 catalyst was calculated by the Gibbs free energy minimization method (Table S7). The equilibrium composition under oxidative condition at 450 °C was compared with that under reductive condition at 850 °C. It was observed that the theoretical time for reductive regeneration is four times longer than that for oxidative regeneration. Therefore, it is inferred that coke hydrogenation rate is limited by thermodynamic equilibrium and requires longer time than coke oxidation.

Raman spectroscopy was also conducted over the 5Mo/H-ZSM-5 catalyst after a 5 H_2 recycle reaction, as represented in Fig. S14 and Table 6. Compared to the recycle reaction with oxidative regeneration (Fig. S11), a higher area ratio of the C—H vibration band (I_{C-H}) was observed. Further, the peak position of the G-band (I_G) shifted to 1560 cm^{-1}, demonstrating that conjugated olefinic coke was formed on the Mo_2C sites during reductive regeneration. Additionally, the trend of the integrated area of the G- to D2-band ratio coincided with that of the L–T/H–T coke ratio, implying that L–T coke is mainly composed of conjugated olefinic carbon and that H–T coke is mainly composed of poly-aromatic carbon.

3.5. DFT study of the catalyst regeneration mechanism

The catalyst regeneration mechanism under oxidative and reductive conditions was investigated by DFT calculations. According to the regenerability test in Fig. 6, removal of Mo-associated coke is crucial for regeneration. Among the plausible coke representatives, naphthalene, a major coke precursor on the acid sites [17], was used as a model compound.

Because the efficient regeneration condition (oxidative regeneration at 450 °C, reductive regeneration at 850 °C) might accompany partial oxidation or hydrogenation of Mo_2C [4,73], the effect of phase transition of Mo species during regeneration was investigated by DFT calculation. Fig. S16(a) compares the relative energy diagrams of naphthalene oxidation on Mo_2C and MoO_3 at 450 °C. Because oxygen

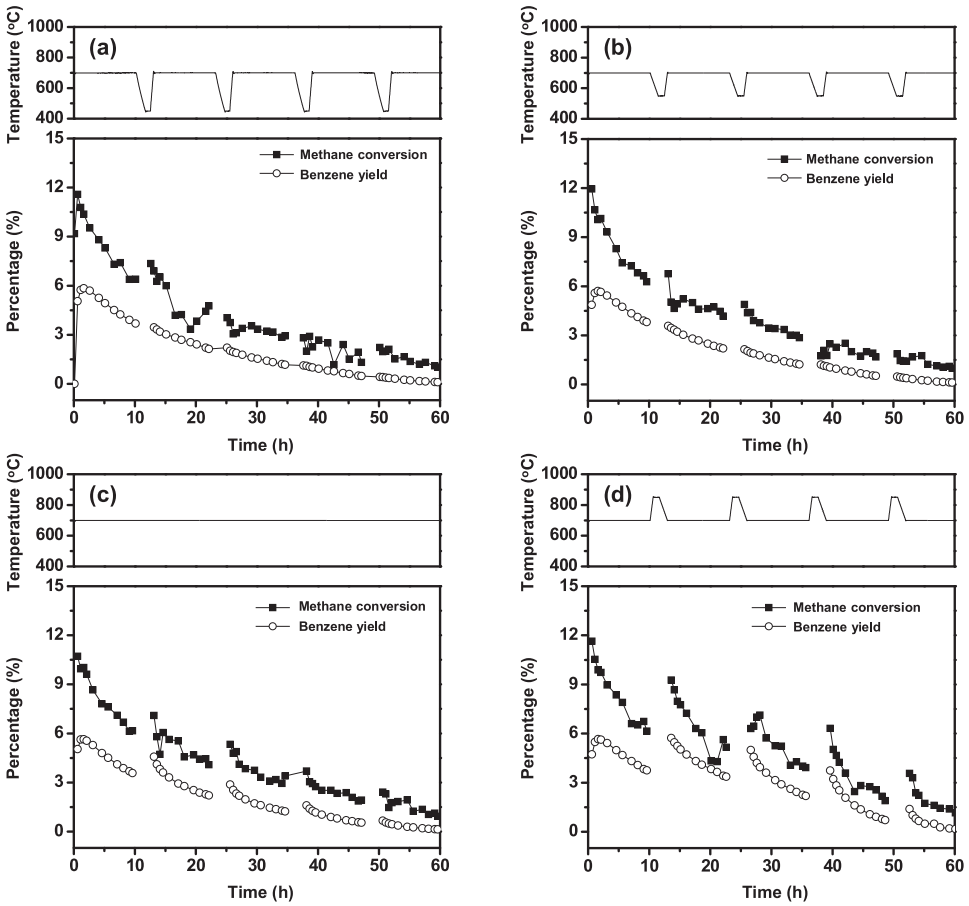

Fig. 9. Methane conversion and benzene yield in the 5 recycle-MDA reaction including reductive regeneration at (a) 450 °C, (b) 550 °C, (c) 700 °C, and (d) 850 °C over 5Mo/H-ZSM-5 catalyst.

adsorption energy on Mo_2C is much higher than that on MoO_3 (Mo_2C: 2.73 eV, MoO_3: −0.65 eV at 450 °C)), naphthalene oxidation on MoO_3 was thermodynamically more favorable than Mo_2C. Considering the TGA results in Fig. 5, it was inferred that Mo_2C oxidation precedes the coke oxidation and MoO_3 formation promotes coke oxidation. Fig. S16(b) compares the relative energy diagrams of naphthalene hydrogenation on Mo_2C and Mo at 850 °C. Unlike the case of naphthalene oxidation, relative energy diagram for naphthalene hydrogenation on Mo_2C and Mo are quite similar. This might be due to the similar hydrogen adsorption energy on Mo_2C and Mo (Mo_2C: −1.00 eV, Mo: −0.84 eV at 850 °C). Rather, the phase transition of Mo_2C to Mo inhibits the naphthalene hydrogenation by increasing hydrogen adsorption energy.

Fig. 11 compares the relative energy diagrams of oxidation and hydrogenation of naphthalene. In the present calculations, Mo oxide and metallic Mo were assumed to be the active species for the oxidative and reductive regenerations, respectively, since transformations of Mo_2C to those species have been reported [4,73]. The Mo oxide cluster was constructed in the form of dimolybdate, while a cluster containing 4 Mo atoms induced from the primary Mo_4C_2 cluster was adopted for metallic Mo, as reported in a previous DFT study [74]. The Mo oxide or metallic Mo cluster was located near the Brønsted acid sites in the ZSM-

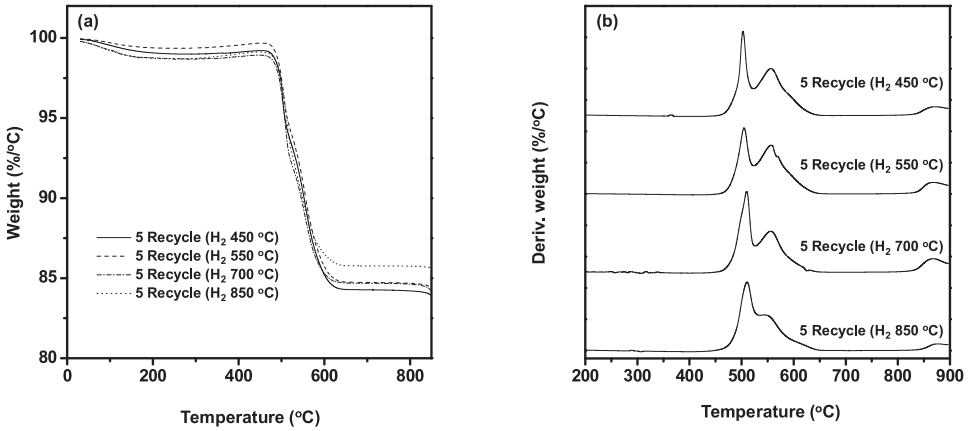

Fig. 10. (a) TG and (b) DTG profiles of used 5Mo/H-ZSM-5 catalysts obtained after a 5 recycle-MDA reaction including reductive regeneration at 450 °C, 550 °C, 700 °C, and 850 °C.

Table 5
Amount of carbon deposition in the 5Mo/H-ZSM-5 catalysts after a 5 cycle-MDA reaction including reductive regeneration.

Catalyst	Carbon deposition (wt%)[a]			
	400–500 °C	500–650 °C	L–T coke/H–T coke ratio	Total
5 Recycle (H_2 450 °C)	5.64	9.26	0.61	14.9
5 Recycle (H_2 550 °C)	4.83	10.07	0.48	14.9
5 Recycle (H_2 700 °C)	6.86	7.34	0.93	14.2
5 Recycle (H_2 850 °C)	7.20	6.10	1.18	13.3

[a] Calculated from deconvoluted peak area of DTG profiles in Fig. 10(b).

5 channel [49]. The electronic energies obtained directly from the DFT calculations and the free energies calculated at the corresponding regeneration temperatures (i.e., 450 °C and 850 °C for the oxidative and reductive regenerations, respectively) are illustrated in Fig. 11.

In the case of oxidation, the full oxidation mechanism for naphthalene is challenging to describe. However, since reaction pathways that proceed via 1,4-napthoquinone are generally accepted [75], we have calculated the energies associated with this type of pathway. For the hydrogenation pathway, tetralin, which is completely saturated on one side, was considered as the key intermediate of this mechanism [76].

The energy diagram shows that oxidation is clearly favorable over hydrogenation. Adsorption of the reaction intermediates calculated by DFT (Fig. S17) shows that the oxygen atom adsorbed on the MoO_3 cluster served as an adsorption site for naphthalene and that oxidation occurred in a stepwise fashion. In contrast, the hydrogenation process exhibited clear thermodynamic barriers, with the formation of partially hydrogenated intermediates. Catalytic regeneration with hydrogen is probably be more effective in removing small and unstable coke species and thus it is important to control kinetics for reductive regeneration. On the other hand, catalytic regeneration with oxygen can successfully remove coke species produced through consecutive reactions (i.e. aromatization, oligomerization, etc) rather than hydrogen.

3.6. XAS study of the Mo/H-ZSM-5 catalysts

Fig. 12 shows the Mo K-edge near-edge spectra of the 5Mo/H-ZSM-5 catalyst after the MDA reaction with oxidative regeneration at 450 °C and 700 °C. For comparison, fresh 5Mo/H-ZSM-5 catalyst and Mo compounds with known structures (i.e., Mo foil, Mo_2C, MoO_3, and $MgMoO_4$) were also considered. In order to investigate the behavior of molybdenum oxide species, the 5Mo/H-ZSM-5 catalyst after 5 recycle reactions were reoxidized at the regeneration temperature and analyzed. Samples containing molybdenum oxide compounds (i.e., fresh 5Mo/H-ZSM, 5 Recycle 450 °C oxidized, and 5 Recycle 700 °C oxidized) exhibited pre-edge features attributable to 1s–4d electronic transitions [77]. Compared with the reference samples, the spectrum of fresh 5Mo/H-ZSM-5 resembled that of MoO_3, whereas the spectra of 5 Recycle O_2 450 °C and 5 Recycle O_2 700 °C resembled that of Mo_2C. This indicates that MoO_3, which formed predominantly in the fresh catalyst, transformed to Mo_2C during the MDA reaction. It was also observed that the

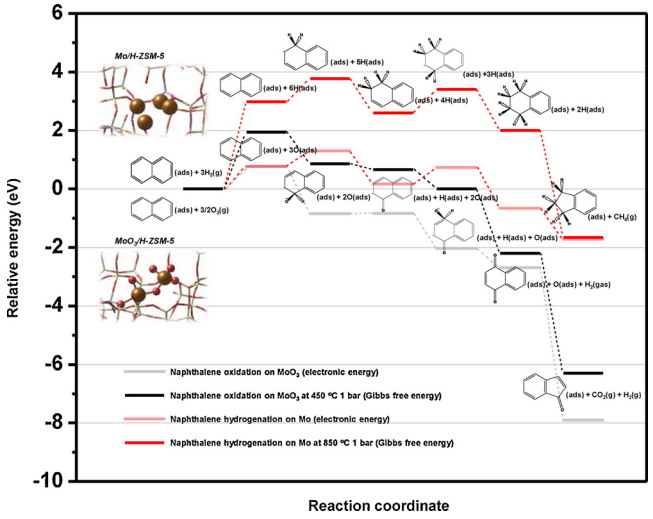

Fig. 11. Relative energy diagram for naphthalene oxidation mechanism over MoO_3/H-ZSM-5 catalyst and naphthalene hydrogenation mechanism over Mo/H-ZSM-5 catalyst.

intensity of the pre-edge peak slightly increased after the regeneration process. This implies that the tetrahedral symmetry of the Mo^{6+} centers increased after regeneration, as evidenced in the pre-edge feature of $MgMoO_4$ [78]. A comparison of the edge energy position of Mo and Mo foil, which provides a measure of the expected oxidation state and extent of aggregation, is represented in Table 7. For these calculations, the edge energy position was defined as the first inflection point beyond the pre-edge features [78]. The edge energy position of fresh 5Mo/H-ZSM-5 catalyst at 20,017.4 eV (> 20,016.3 eV) implies that Mo species were dispersed in the form of MoO_3 and MoO_4^{2-}. In addition, the phase transition of molybdenum oxide to molybdenum carbide is confirmed by the change of the edge energy position after the reaction. Interestingly, the molybdenum edge energy position of the catalyst after regeneration at 700 °C (20,001.0 eV) was lower than that of the catalyst after regeneration at 450 °C (20,001.5 eV). Because the edge energy position decreases with increasing molybdenum domain size [79], these results reveal that the size of molybdenum oxide and molybdenum carbide increased with increasing regeneration temperature.

The k^3-weighted EXAFS profiles of the 5Mo/H-ZSM-5 catalyst after the 5-cycle reaction are shown in Fig. S18(b). The radial structure functions were obtained by Fourier transform of the X-ray absorption data in the post-edge region. For comparison, Mo-containing compounds with known structures are also shown in Fig. S18(a). The radial functions of fresh 5Mo/H-ZSM-5 retained peaks for Mo-O (1.2 Å) and Mo-Mo (3.1 Å), resembling the profile of bulk MoO_3 [80]. The relatively low intensity of the Mo-Mo peak compared to MoO_3 was observed in the fresh 5Mo/H-ZSM-5 catalyst and is indicative of a high Mo dispersion. However, the 5 Recycle O_2, 450 °C and 5 Recycle O_2, 700 °C catalysts exhibited a single sharp peak for Mo-O coordination and the peak for Mo-Mo decreased, which resembles the EXAFS profile of $MgMoO_4$. This implies that MoO_4^{2-} with a tetrahedral symmetry converted from MoO_3 crystallites with octahedral symmetry at the

Table 6
Characteristic fraction of deconvoluted area of bands assigned in the Raman spectra of 5Mo/H-ZSM-5 catalysts after a 5 cycle-MDA reaction including reductive regeneration.

Catalyst	I_{C-H} (%)[a]	I_{D1} (%)[a]	I_{D3} (%)[a]	I_G (%)[a]	I_{D2} (%)[a]	P_{D2} (cm^{-1})	I_G/I_{D2}
5 Recycle (H_2 450 °C)	12.1	38.1	13.0	15.3	21.4	1603	0.71
5 Recycle (H_2 550 °C)	13.1	39.0	13.2	13.3	21.4	1601	0.62
5 Recycle (H_2 700 °C)	14.5	35.5	15.5	16.4	18.1	1602	0.91
5 Recycle (H_2 850 °C)	12.4	38.2	15.8	16.3	17.3	1604	0.94

[a] Calculated from deconvoluted peak area of Raman spectra in Fig. S14.

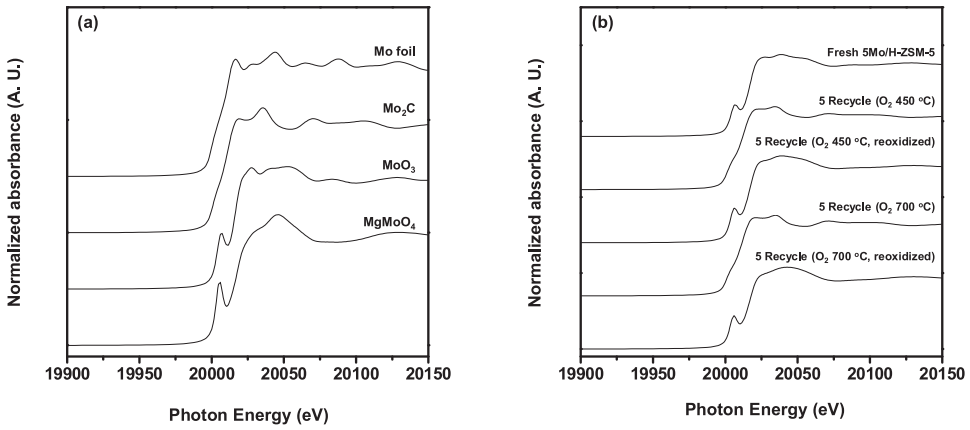

Fig. 12. Mo K-edge near-edge spectra of (a) Mo-containing references and (b) 5Mo/H-ZSM-5 catalyst before and after 5 recycle-MDA reaction including the oxidative regeneration process at 450 °C and 700 °C.

Table 7
Edge energy positions of Mo in the reference samples and 5Mo/H-ZSM-5 catalyst before and after a 5 cycle-MDA reaction including oxidative regeneration.

Sample	Edge energy position (E_0)/eV[a]
Mo_2C	20001.1
MoO_3	20016.3
$MgMoO_4$	20017.9
Fresh 5Mo/H-ZSM-5	20017.4
5 Recycle (O_2 450 °C)	20001.5
5 Recycle (O_2 450 °C, reoxidized)	20017.1
5 Recycle (O_2 700 °C)	20001.0
5 Recycle (O_2 700 °C, reoxidized)	20017.3

[a] Edge energy position was defined as the first inflection point beyond the pre-edge features of XANES profiles in Fig. 12.

initial stage of the reaction [77], and it is reversibly recovered during the oxidative regeneration process. Therefore, the increase of catalytic activity after the first oxidative regeneration at 450 °C may be attributed to the increase of Mo dispersion through the formation of $(MoO_4)^{2-}$. Although a single sharp peak for Mo-O coordination was noticeable at high regeneration temperature, the peak intensity Mo-(C)-Mo peak increased with increasing regeneration temperature, which is indicative of Mo_2C sintering. This might be due to the increased $(MoO_x)_n$ oligomerization on external surface of H-ZSM-5 during oxidative regeneration at 700 °C [52].

4. Conclusion

A series of Mo/H-ZSM-5 catalysts with different Mo loadings (1, 3, 5, 7 wt%) were prepared and applied to non-oxidative dehydroaromatization of methane at 700 °C. It was observed that 5 wt% is an optimal Mo loading for methane dehydroaromatization. Mechanistic studies demonstrated that excessively high acid site/Mo_2C site ratio induced deactivation by coke formation. The 5Mo/H-ZSM-5 catalyst was applied to reaction-regeneration cycles under both oxidative and reductive regeneration conditions of 450–850 °C. It was revealed that oxidative regeneration at 450 °C is the most efficient for maintaining catalytic activity and stability. The TGA and Raman spectroscopic results showed that L–T and H–T coke are mainly derived from Mo-associated graphite coke and acid site-associated poly-aromatic coke, respectively. It was found that removal of Mo-associated coke is crucial to regenerate the catalyst. The selective recovery of Brønsted acid sites near Mo sites other than isolated acid sites is sufficient to restore the catalytic activity in terms of benzene formation. Coke oxidation and hydrogenation models of the Mo/H-ZSM-5 catalyst were constructed by density functional theory and their corresponding relative energy diagrams were calculated; relative to coke hydrogenation on Mo at 850 °C, coke oxidation on MoO_3 at 450 °C is thermodynamically favorable. The phase transition of molybdenum species during the reaction-regeneration cycles was investigated by XAS analyses. In particular, the XANES and EXAFS results revealed that low regeneration temperatures induced MoO_4^{2-} formation with increased dispersion, whereas high regeneration temperatures caused MoO_4^{2-} oligomerization on the external surface of the zeolite, resulting in Mo_2C sintering. Consequently, it was found that the removal of Mo-associated coke while maintaining a high dispersion of Mo_2C is required for effective catalyst regeneration in the MDA reaction.

Acknowledgements

This research was supportedby C1 Gas Refinery Program through the National Research Foundation of Korea (NRF) funded by the Ministry of Science, ICT & Future Planning (NRF-2017M3D3A1A01037001). This research was further financially supported by the KRICT big project (SI1801-06) of the Korea Research Institute of Chemical Technology. We also appreciate an additional support from the Supercomputing Center at the Korea Institute of Science and Technology Information (KISTI), with supercomputing resources and technical support (KSC-2016-C1-0014).

Appendix A. Supplementary data

Supplementary material related to this article can be found, in the online version, at doi:https://doi.org/10.1016/j.apcatb.2018.09.042.

References

[1] S. Ma, X. Guo, L. Zhao, S. Scott, X. Bao, Recent progress in methane dehydroaromatization: from laboratory curiosities to promising technology, J. Energy Chem. 22 (2013) 1–20.
[2] A. Galadima, O. Muraza, Revisiting the oxidative coupling of methane to ethylene in the golden period of shale gas: a review, J. Ind. Eng. Chem. 37 (2016) 1–13.
[3] H. Burghgraef, A.P.J. Jansen, R.A. van Santen, Methane activation and dehydrogenation on nickel and cobalt: a computational study, Surf. Sci. 324 (1995) 345–356.
[4] Y. Xu, X. Bao, L. Lin, Direct conversion of methane under nonoxidative conditions, J. Catal. 216 (2003) 386–395.
[5] D.A. Hickman, L.D. Schmidt, Production of syngas by direct catalytic oxidation of methane, Science 259 (1993) 343–346.
[6] E. Iglesia, Design, synthesis, and use of cobalt-based Fischer-Tropsch synthesis catalysts, Appl. Catal. Gen. 161 (1997) 59–78.
[7] X. Guo, G. Fang, G. Li, H. Ma, H. Fan, L. Yu, C. Ma, X. Wu, D. Deng, M. Wei, D. Tan, R. Si, S. Zhang, J. Li, L. Sun, Z. Tang, X. Pan, X. Bao, Direct, nonoxidative conversion of methane to ethylene, aromatics, and hydrogen, Science 344 (2014) 616–619.
[8] G.E. Keller, M.M. Bhasin, Synthesis of ethylene via oxidative coupling of methane. I. Determination of active catalysts, J. Catal. 73 (1982) 9–19.
[9] Y. Xu, L. Lin, Recent advances in methane dehydro-aromatization over transition metal ion-modified zeolite catalysts under non-oxidative conditions, Appl. Catal.

Gen. 188 (1999) 53–67.
[10] L. Wang, L. Tao, M. Xie, G. Xu, J. Huang, Y. Xu, Dehydrogenation and aromatization of methane under non-oxidizing conditions, Catal. Lett. 21 (1993) 35–41.
[11] M.V. Luzgin, V.A. Rogov, S.S. Arzumanov, A.V. Toktarev, A.G. Stepanov, V.N. Parmon, Understanding methane aromatization on a Zn-modified high-silica zeolite, Angew. Chem. Int. Ed. 47 (2008) 4559–4562.
[12] L. Wang, R. Ohnishi, M. Ichikawa, Selective dehydroaromatization of methane toward benzene on Re/HZSM-5 catalysts and effects of CO/CO_2 addition, J. Catal. 190 (2000) 276–283.
[13] Y. Shu, R. Ohnishi, M. Ichikawa, Improved methane dehydrocondensation reaction on HMCM-22 and HZSM-5 supported rhenium and molybdenum catalysts, Appl. Catal. Gen. 252 (2003) 315–329.
[14] P. He, R. Gatip, M. Yung, H. Zeng, H. Song, Co-aromatization of olefin and methane over Ag-Ga/ZSM-5 catalyst at low temperature, Appl. Catal. B: Environ. 211 (2017) 275–288.
[15] A. Wang, P. He, M. Yung, H. Zeng, H. Qian, H. Song, Catalytic co-aromatization of ethanol and methane, Appl. Catal. B: Environ. 198 (2016) 480–492.
[16] P. He, J. Jarvis, S. Meng, A. Wang, S. Kou, R. Gatip, M. Yung, Co-aromatization of methane with olefins: the role of inner pore and external surface catalytic sites, Appl. Catal. B: Environ. 234 (2018) 234–246.
[17] S. Liu, L. Wang, R. Ohnishi, M. Ichikawa, Bifunctional catalysis of Mo/HZSM-5 in the dehydroaromatization of methane to benzene and naphthalene XAFS/TG/DTA/MASS/FTIR characterization and supporting effects, J. Catal. 181 (1999) 175–188.
[18] H. Liu, X. Bao, Y. Xu, Methane dehydroaromatization under nonoxidative conditions over Mo/HZSM-5 catalysts: identification and preparation of the Mo active species, J. Catal. 239 (2006) 441–450.
[19] H. Zheng, D. Ma, X. Bao, Z.H. Jian, H.K. Ja, Y. Wang, C.H.F. Peden, Direct observation of the active center for methane dehydroaromatization using an ultrahigh field 95Mo NMR spectroscopy, J. Am. Chem. Soc. 130 (2008) 3722–3723.
[20] L. Chen, L. Lin, Z. Xu, T. Zhang, X. Li, Promotional effect of Pt on non-oxidative methane transformation over Mo-HZSM-5 catalyst, Catal. Lett. 39 (1996) 169–172.
[21] V. Abdelsayed, D. Shekhawat, M.W. Smith, Effect of Fe and Zn promoters on Mo/HZSM-5 catalyst for methane dehydroaromatization, Fuel 139 (2015) 401–410.
[22] B. Liu, Y. Yang, A. Sayari, Non-oxidative dehydroaromatization of methane over Ga-promoted Mo/HZSM-5-based catalysts, Appl. Catal. Gen. 214 (2001) 95–102.
[23] B.S. Liu, L. Jiang, H. Sun, C.T. Au, XPS, XAES, and TG/DTA characterization of deposited carbon in methane dehydroaromatization over Ga-Mo/ZSM-5 catalyst, Appl. Surf. Sci. 253 (2007) 5092–5100.
[24] Y. Xu, J. Wang, Y. Suzuki, Z.G. Zhang, Effect of transition metal additives on the catalytic stability of Mo/HZSM-5 in the methane dehydroaromatization under periodic CH_4-H_2 switch operation at 1073 K, Appl. Catal. Gen. 409–410 (2011) 181–193.
[25] C.H.L. Tempelman, V.O. De Rodrigues, E.R.H. Van Eck, P.C.M.M. Magusin, E.J.M. Hensen, Desilication and silylation of Mo/HZSM-5 for methane dehydroaromatization, Microporous Mesoporous Mater. 203 (2015) 259–273.
[26] A. Martínez, E. Peris, Non-oxidative methane dehydroaromatization on Mo/HZSM-5 catalysts: tuning the acidic and catalytic properties through partial exchange of zeolite protons with alkali and alkaline-earth cations, Appl. Catal. Gen. 515 (2016) 32–44.
[27] N. Kosinov, F.J.A.G. Coumans, G. Li, E. Uslamin, B. Mezari, A.S.G. Wijpkema, E.A. Pidko, E.J.M. Hensen, Stable Mo/HZSM-5 methane dehydroaromatization catalysts optimized for high-temperature calcination-regeneration, J. Catal. 346 (2017) 125–133.
[28] P.L. Tan, Y.L. Leung, S.Y. Lai, C.T. Au, Methane aromatization over 2 wt% Mo/HZSM-5 in the presence of O_2 and NO, Catal. Lett. 78 (2002) 251–258.
[29] S. Liu, L. Wang, R. Ohnishi, Bifunctional catalysis of Mo/HZSM-5 in the dehydroaromatization of methane with CO/CO_2 to benzene and naphthalene, Kinet. Catal. 41 (2000) 148–160.
[30] H. Ma, R. Ohnishi, M. Ichikawa, Highly stable performance of methane dehydroaromatization on Mo/HZSM-5 catalyst with a small amount of H_2 addition into methane feed, Catal. Lett. 89 (2003) 143–146.
[31] Y. Song, Y. Xu, Y. Suzuki, H. Nakagome, X. Ma, Z.G. Zhang, The distribution of coke formed over a multilayer Mo/HZSM-5 fixed bed in H_2 co-fed methane aromatization at 1073 K: exploration of the coking pathway, J. Catal. 330 (2015) 261–272.
[32] N. Kosinov, F.J.A.G. Coumans, E. Uslamin, F. Kapteijn, E.J.M. Hensen, Selective coke combustion by oxygen pulsing during Mo/ZSM-5-catalyzed methane dehydroaromatization, Angew. Chem. Int. Ed. 55 (2016) 15086–15090.
[33] A.C.C. Rodrigues, J.L.F. Monteiro, The use of CH_4/H_2 cycles on dehydroaromatization of methane over MoMCM-22, Catal. Commun. 9 (2008) 1060–1065.
[34] Y. Shu, H. Ma, R. Ohnishi, M. Ichikawa, Highly stable performance of catalytic methane dehydrocondensation towards benzene on Mo/HZSM-5 by a periodic switching treatment with H_2 and CO_2, Chem Commun. (2003) 86–87.
[35] Y. Xu, J. Lu, J. Wang, Y. Suzuki, Z.G. Zhang, The catalytic stability of Mo/HZSM-5 in methane dehydroaromatization at severe and periodic CH_4-H_2 switch operating conditions, Chem. Eng. J. 168 (2011) 390–402.
[36] M.T. Portilla, F.J. Llopis, C. Martínez, Non-oxidative dehydroaromatization of methane: an effective reaction-regeneration cyclic operation for catalyst life extension, Catal. Sci. Technol. 5 (2015) 3806–3821.
[37] Y. Lu, Z. Xu, Z. Tian, Z. Tao, L. Lin, Methane aromatization in the absence of an added oxidant and the bench scale reaction test, Catal. Lett. 62 (1999) 215–220.
[38] W.E. Farneth, R.J. Gorte, Methods for characterizing zeolite acidity, Chem. Rev. 95 (1995) 615–635.
[39] R.J. Gorte, What do we know about the acidity of solid acids? Catal. Lett. 62 (1999) 1–13.
[40] B. Ravel, M. Newville, ATHENA, ARTEMIS, HEPHAESTUS: data analysis for x-ray absorption spectroscopy using IFEFFIT, J. Synchrotron Radiat. 12 (2005) 537–541.
[41] G. Kresse, J. Hafner, Ab initio molecular-dynamics simulation of the liquid-metal-amorphous-semiconductor transition in germanium, Phys. Rev. B 49 (1994) 14251–14269.
[42] G. Kresse, J. Furthmüller, Efficiency of ab-initio total energy calculations for metals and semiconductors using a plane-wave basis set, Comput. Mater. Sci. 6 (1996) 15–50.
[43] B. Hammer, L.B. Hansen, J.K. Nørskov, Improved adsorption energetics within density-functional theory using revised Perdew–Burke–Ernzerhof functionals, Phys. Rev. B 59 (1999) 7413–7421.
[44] M. Dion, H. Rydberg, E. Schröder, D.C. Langreth, B.I. Lundqvist, Van der Waals density functional for general geometries, Phys. Rev. Lett. 92 (2004) 22–25.
[45] J. Klime, D.R. Bowler, A. Michaelides, Van der Waals density functionals applied to solids, Phys. Rev. B: Condens. Matter Mater. Phys. 83 (2011) 1–13.
[46] G. Román-Pérez, J.M. Soler, Efficient implementation of a van der Waals density functional: application to double-wall carbon nanotubes, Phys. Rev. Lett. 103 (2009) 1–4.
[47] K. Lee, É.D. Murray, L. Kong, B.I. Lundqvist, D.C. Langreth, Higher-accuracy van der Waals density functional, Phys. Rev. B: Condens. Matter Mater. Phys. 82 (2010) 3–6.
[48] C.J. Cramer, Essentials of Computational Chemistry: Theories and Models, John Wiley & Sons, 2013.
[49] W. Ding, S. Li, G.D. Meitzner, E. Iglesia, Methane conversion to aromatics on Mo/H-ZSM5: structure of molybdenum species in working catalysts, J. Phys. Chem. B 105 (2001) 506–513.
[50] N. Kosinov, F.J.A.G. Coumans, E.A. Uslamin, A.S.G. Wijpkema, B. Mezari, E.J.M. Hensen, Methane dehydroaromatization by Mo/HZSM-5: mono- or bifunctional catalysis? ACS Catal. 7 (2017) 520–529.
[51] J.P. Tessonnier, B. Louis, S. Walspurger, J. Sommer, M.J. Ledoux, C. Pham-Huu, Quantitative measurement of the Brönsted acid sites in solid acids: toward a single-site design of Mo-modified ZSM-5 zeolite, J. Phys. Chem. B 110 (2006) 10390–10395.
[52] W. Li, G.D. Meitzner, R.W. Borry, E. Iglesia, Raman and X-ray absorption studies of Mo species in Mo/H-ZSM5 catalysts for non-oxidative CH_4 reactions, J. Catal. 191 (2000) 373–383.
[53] J. Bedard, D.Y. Hong, A. Bhan, CH_4 dehydroaromatization on Mo/H-ZSM-5: 1. Effects of co-processing H_2 and CH_3COOH, J. Catal. 306 (2013) 58–67.
[54] K.S. Wong, J.W. Thybaut, E. Tangstad, M.W. Stöcker, G.B. Marin, Methane aromatisation based upon elementary steps: kinetic and catalyst descriptors, Microporous Mesoporous Mater. 164 (2012) 302–312.
[55] Z.R. Ismagilov, E.V. Matus, L.T. Tsikoza, Direct conversion of methane on Mo/ZSM-5 catalysts to produce benzene and hydrogen: achievements and perspectives, Energy Environ. Sci. 1 (2008) 526–541.
[56] E.V. Matus, I.Z. Ismagilov, O.B. Sukhova, V.I. Zaikovskii, L.T. Tsikoza, Z.R. Ismagilov, J.A. Moulijn, Study of methane dehydroaromatization on impregnated Mo/ZSM-5 catalysts and characterization of nanostructured molybdenum phases and carbonaceous deposits, Ind. Eng. Chem. Res. 46 (2007) 4063–4074.
[57] J.J. Spivey, G. Hutchings, Catalytic aromatization of methane, Chem. Soc. Rev. 43 (2014) 792–803.
[58] Y. Song, Y. Xu, Y. Suzuki, H. Nakagome, Z.G. Zhang, A clue to exploration of the pathway of coke formation on Mo/HZSM-5 catalyst in the non-oxidative methane dehydroaromatization at 1073 K, Appl. Catal. Gen. 482 (2014) 387–396.
[59] J. Bedard, D.-Y. Hong, A. Bhan, C to H effective ratio as a descriptor for co-processing light oxygenates and CH_4 on Mo/H-ZSM-5, RSC Adv. 4 (2014) 49446–49448.
[60] J. Bedard, D.-Y. Hong, A. Bhan, Co-processing CH_4 and oxygenates on Mo/H-ZSM-5: 2. CH_4—CO_2 and CH_4—HCOOH mixtures, Phys. Chem. Chem. Phys. 15 (2013) 12173.
[61] N. Kosinov, A.S.G. Wijpkema, E. Uslamin, R. Rohling, F. Coumans, B. Mezari, A. Parastaev, A.S. Poryvaev, M.V. Fedin, E.A. Pidko, E.J.M. Hensen, Confined carbon mediating dehydroaromatization of methane over Mo/ZSM-5, Angew. Chem. Int. Ed. 57 (2018) 1016–1020.
[62] J. Gao, Y. Zheng, J.-M. Jehng, Y. Tang, S.G. Podkolzin, I.E. Wachs, Identification of molybdenum oxide nanostructures on zeolites for natural gas conversion, Science 348 (2015) 686–690.
[63] H. Liu, W. Shen, X. Bao, Y. Xu, Methane dehydroaromatization over Mo/HZSM-5 catalysts: the reactivity of MoC_x species formed from MoO_x associated and non-associated with Brönsted acid sites, Appl. Catal. Gen. 295 (2005) 79–88.
[64] H. Liu, L. Su, H. Wang, W. Shen, X. Bao, Y. Xu, The chemical nature of carbonaceous deposits and their role in methane dehydro-aromatization on Mo/MCM-22 catalysts, Appl. Catal. Gen. 236 (2002) 263–280.
[65] P. Castaño, G. Elordi, M. Olazar, A.T. Aguayo, B. Pawelec, J. Bilbao, Insights into the coke deposited on HZSM-5, Hβ and HY zeolites during the cracking of polyethylene, Appl. Catal. B: Environ. 104 (2011) 91–100.
[66] C. Li, P.C. Stair, Ultraviolet Raman spectroscopy characterization of coke formation in zeolites, Catal. Today 33 (1997) 353–360.
[67] S.J. Ardakani, X. Liu, K.J. Smith, Hydrogenation and ring opening of naphthalene on bulk and supported Mo_2C catalysts, Appl. Catal. Gen. 324 (2007) 9–19.
[68] J.W. Ward, The nature of active sites on zeolites VI. The influence of calcination temperature on the structural hydroxyl groups and acidity of stabilized hydrogen Y zeolite, J. Catal. 11 (1968) 251–258.
[69] C.H.L. Tempelman, E.J.M. Hensen, On the deactivation of Mo/HZSM-5 in the methane dehydroaromatization reaction, Appl. Catal. B: Environ. 176–177 (2015) 731–739.
[70] Y. Yamamoto, Y. Ogawa, H.T. Ma, M. Kuramoto, Development of MTB process key technologies: a clean process that produces plastics from greenhouse gases, Meiden

Rev. 151 (2011) 35–39.
[71] A. Martínez, E. Peris, M. Derewinski, A. Burkat-dulak, Improvement of catalyst stability during methane dehydroaromatization (MDA) on Mo/HZSM-5 comprising intracrystalline mesopores, Catal. Today 169 (2011) 75–84.
[72] H.G. Karge, W. Nieβen, H. Bludau, In-situ FTIR measurements of diffusion in coking zeolite catalysts, Appl. Catal. Gen. 146 (1996) 339–349.
[73] K. Oshikawa, M. Nagai, S. Omi, Characterization of molybdenum carbides for methane reforming by TPR, XRD, and XPS, J. Phys. Chem. B 105 (2001) 9124–9131.
[74] J. Gao, Y. Zheng, G.B. Fitzgerald, J. De Joannis, Y. Tang, I.E. Wachs, S.G. Podkolzin, Structure of Mo_2C_x and Mo_4C_x molybdenum carbide nanoparticles and their anchoring sites on zsm-5 zeolites, J. Phys. Chem. C 118 (2014) 4670–4679.
[75] X. Zhang, S. Shen, K. Hidajat, S. Kawi, L.E. Yu, K.Y.S. Ng, Naphthalene oxidation over 1% Pt and 5% Co/Y-Al_2O_3 catalysts : reaction intermediates and possible pathways, Catal. Lett. 96 (2004) 87–96.
[76] H. Du, C. Fairbridge, H. Yang, Z. Ring, The chemistry of selective ring-opening catalysts, Appl. Catal. Gen. 294 (2005) 1–21.
[77] I. Lezcano-González, R. Oord, M. Rovezzi, P. Glatzel, S.W. Botchway, B.M. Weckhuysen, A.M. Beale, Molybdenum speciation and its impact on catalytic activity during methane dehydroaromatization in zeolite ZSM-5 as revealed by operando X-ray methods, Angew. Chem. Int. Ed. 55 (2016) 5215–5219.
[78] H.S. Lacheen, E. Iglesia, Stability, structure, and oxidation state of Mo/H-ZSM-5 catalysts during reactions of CH_4 and CH_4-CO_2 mixtures, J. Catal. 230 (2005) 173–185.
[79] R.S. Weber, Effect of local structure on the UV-visible absorption edges of molybdenum oxide clusters and supported molybdenum oxides, J. Catal. 151 (1995) 470–474.
[80] H. Aritani, H. Shibasaki, H. Orihara, A. Nakahira, Methane dehydroaromatization over Mo-modified H-MFI for gas to liquid catalysts, J. Environ. Sci. 21 (2009) 736–740.